CHEMISTRY

Guanidinium-based covalent organic framework membrane for single-acid recovery

Qing-Wei Meng[1]†, Shaochun Wu[1]†, Mingjie Liu[2,3], Qing Guo[1], Weipeng Xian[1], Xiuhui Zuo[1], Sai Wang[1], Hong Yin[1], Shengqian Ma[4]*, Qi Sun[1]*

Acids are extensively used in contemporary industries. However, time-consuming and environmentally unfriendly processes hinder single-acid recovery from wastes containing various ionic species. Although membrane technology can overcome these challenges by efficiently extracting analytes of interest, the associated processes typically exhibit inadequate ion-specific selectivity. In this regard, we rationally designed a membrane with uniform angstrom-sized pore channels and built-in charge-assisted hydrogen bond donors that preferentially conducted HCl while exhibiting negligible conductance for other compounds. The selectivity originates from the size-screening ability of angstrom-sized channels between protons and other hydrated cations. The built-in charge-assisted hydrogen bond donor enables the screening of acids by exerting host-guest interactions to varying extents, thus acting as an anion filter. The resulting membrane exhibited exceptional permeation for protons over other cations and for Cl^- over SO_4^{2-} and $H_nPO_4^{(3-n)-}$ with selectivities up to 4334 and 183, respectively, demonstrating prospects for HCl extraction from waste streams. These findings will aid in designing advanced multifunctional membranes for sophisticated separation.

INTRODUCTION

HCl is a critical chemical in contemporary industrial applications because of its widespread use in steel processing, electroplating, and mining (1–4). However, the discharge of large amounts of acidic wastewater from various industries causes severe environmental pollution. Although neutralization is an effective method for treating acids, the disposal of highly concentrated brine in an environmentally friendly manner is challenging (5). Membrane technology is a potential alternative for pollutant removal and is used efficiently in numerous water purification processes (6–24). However, a substantial distinction between specific acid recovery and contaminant removal is required to enable both anion- and cation-specific selectivity due to the presence of various concentrated ionic species in the waste. Typical ions in acidic wastewater include Mg^{2+}, Na^+, Ca^{2+}, Fe^{2+}, Al^{3+}, Cl^-, SO_4^{2-}, and $H_nPO_4^{(3-n)-}$, with conventional proton production focusing only on multivalent cation removal. Cationic membranes that are impermeable to multivalent metal ions because of Donnan exclusion while allowing the permeation of highly mobile protons have been successfully applied for the selective recovery of H^+ from wastes containing Fe^{2+} and Ti^{4+} ions (25–27). However, these membranes exhibit negligible anion selectivity, which hampers the production of a single acid. Furthermore, charge repulsion during these separation processes leads to the slow transport of protons when approaching an anion exchange membrane. Hence, developing advanced separation layers is essential to diversifying the availability of high-purity acids.

The efficient transportation of target compounds via the synergistic integration of multiple separation mechanisms underpins fundamental cellular processes (28–32). In biological ion filters, efficient anion screening is accomplished by inducing directional hydrogen bonding interactions with the aid of ionic interactions (33, 34). Hence, efforts to chemically mimic these associations have led to the development of numerous anion receptors, in which the robustness of the recognition pattern of hydrogen bonding interactions is reinforced or supplemented when hydrogen bond donors and acceptors are ionic, enabling high anion screening ability (35–39). Molecular sieving can provide an efficient pathway for the extraction of protons from various cations because of the smaller size of the protons compared to other hydrated cations (40–42). Therefore, we designed an anion filter with precise size-screening properties to facilitate specific acid transport. Charge-assisted hydrogen bond donors were introduced into the angstrom-sized membrane channels to confer both anionic and proton selectivity. The resulting membrane preferentially conducts HCl over other compounds with a selectivity substantially surpassing that of commercial ionic membranes and reported systems (Fig. 1 and table S1). The fundamental impacts of membrane pore size and pore environment on concentration gradient–driven ion transport were elucidated by combining experimental and computational results. The findings of this study may enlighten the design of advanced membranes for applications requiring the extraction of target species.

RESULTS

Membrane fabrication and characterization

Guanidine is a fundamental compound found in nature, and has been extensively used as a hydrogen bond donor. In addition, the high pK_a (where K_a is the acid dissociation constant) of guanidine (13.6) allows the recognition of acids via charge-assisted hydrogen bonding interactions (43). To test this hypothesis, a guanidinium-

[1]Zhejiang Provincial Key Laboratory of Advanced Chemical Engineering Manufacture Technology, College of Chemical and Biological Engineering, Zhejiang University, Hangzhou 310027, China. [2]Key Laboratory of Biomass Chemical Engineering of Ministry of Education, College of Chemical and Biological Engineering, Zhejiang University, Hangzhou 310027, China. [3]Institute of Zhejiang University-Quzhou, Quzhou 324000, China. [4]Department of Chemistry, University of North Texas, 1508 W Mulberry St, Denton, TX 76201, USA.
*Corresponding author. Email: sunqichs@zju.edu.cn (Q.S.); shengqian.ma@unt.edu (S.M.)
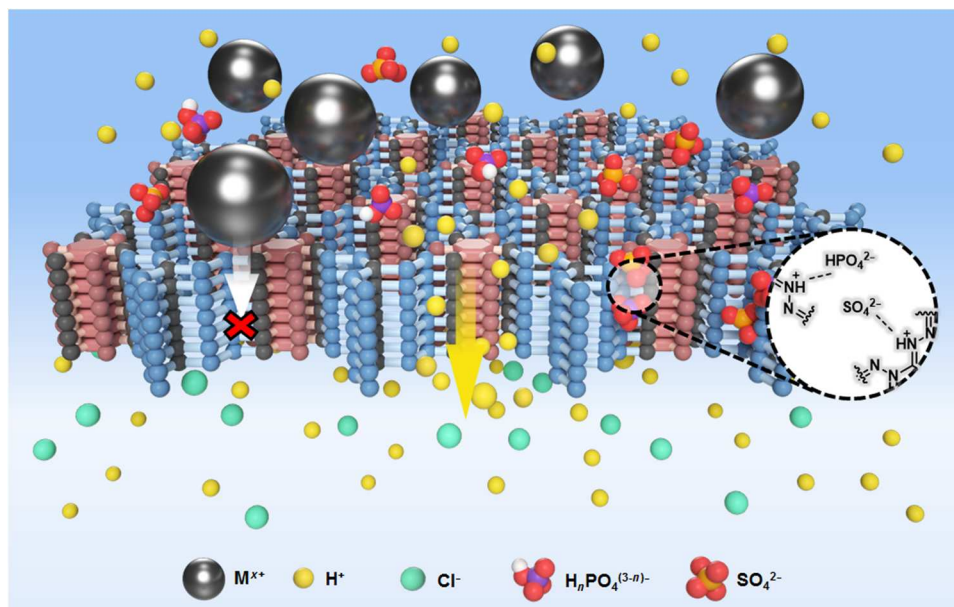†These authors contributed equally to this work.

Fig. 1. Multifunctional COF membrane for HCl extraction. Conceptual schematic illustration of a membrane with angstrom-sized pore channel and built-in charge-assisted hydrogen bond donors to confer both anion and proton selectivity.

containing covalent organic framework (COF) membrane with angstrom-sized channels was fabricated according to our previously reported method, with a slight modification, via the interfacial polymerization of 1,3,5-triformylphloroglucinol (Tp) and triamino-guanidine hydrochloride (Tag) on a polyacrylonitrile (PAN) support (fig. S1) (*44*). The integrity of TpTag-COF/PAN was confirmed using scanning electron microscopy (SEM) images, which revealed a continuous and crack-free COF layer on the PAN layer with a thickness of approximately 38 nm (figs. S2 and S3). Given that the COF active layer is very thin, its powder x-ray diffraction (PXRD) peaks were substantially suppressed by the PAN support. Theoretical simulation was conducted on the basis of the PXRD analysis of the free-standing membrane after dissolving the PAN. TpTag-COF/PAN exhibited a pore size of 7.5 Å along the *c* axis (figs. S4 to S6), while the guanidinium moieties were nearly eclipsed and aligned in the one-dimensional pore channels with a distance of 3.4 Å. N_2 sorption isotherms of TpTag-COF obtained at 77 K validated the pore structure of the membrane. A Brunauer-Emmett-Teller surface area of 286 m^2 g^{-1} with a pore size distribution centered at 7.5 Å was obtained, which is consistent with the simulated eclipsed AA stacking structure. High-resolution transmission EM showed the existence of porosity with a pore size of approximately 7.5 Å (fig. S8). Dye exclusion experiments confirmed the compactness of the TpTag-COF/PAN (fig. S9). The zeta potential of TpTag-COF/PAN decreased from 5.1 to −7.6 mV in response to the increase in the pH of the solution from 1 to 11 (fig. S10).

Investigation of transmembrane ion transport

Our previous study showed that strong hydrogen bonding interactions between the guanidinium moieties on the framework and Cl⁻ ions lead to a substantial degree of charge transfer at the interface. The electrostatic field emanates from the polarization of Cl⁻ ions to the surroundings, resulting in the negative interface. The cationic TpTag-COF/PAN membrane displayed an overscreened surface

charge, favoring the transport of K⁺ over Cl⁻ (*44*). Reversal currents (I_r) in asymmetric acid solutions were measured to validate the preferred transport of protons over counterions. Given that the concentration difference drives both protons and counterions from the high concentration side to the low concentration area to achieve equilibrium, the sign of the current at zero voltage indicates whether the majority carriers are protons (positive current) or their counterions (negative current). Current-voltage relation (*I-V*) plots obtained at concentration differences of 1000, 100, and 10 revealed that the currents at zero voltage were always positive, independent of the absolute HCl, H_2SO_4, or H_3PO_4 concentrations, confirming the higher activity of TpTag-COF/PAN–mediated transport of protons than that of the corresponding counterions (Fig. 2A and fig. S11). Considering excellent permselectivity, the transport activities of other monovalent cations across TpTag-COF/PAN were investigated. Reversal potentials (V_r) were recorded in unsymmetrical baths (*cis* chamber = 0.1 M LiCl, NaCl, or KCl and *trans* chamber = 0.1 M HCl, whereby *cis* chamber refers to the one facing the COF layer). V_r values were −93.3, −101.9, and −115.7 mV for KCl, NaCl, and LiCl, corresponding to H⁺/M⁺ permeability values of 38, 53, and 91, respectively, which were calculated using the Goldman-Hodgkin-Katz equation (*45, 46*). These results provide compelling evidence of the higher proton selectivity of TpTag-COF/PAN than that of the other cations (Fig. 2B). Concurrently, the simulation results revealed that guanidinium exhibits different charge-assisted hydrogen bonding interaction strengths with various anions, thereby suggesting TpTag-COF as a potential anion filter (fig. S12).

To evaluate the anion-screening ability of the designed membrane, the acid conduction across TpTag-COF/PAN was measured by recording the *I-V* curves for HCl, H_2SO_4, and H_3PO_4 (0.1 M) (the acid concentrations described here are based on the whole molecule, if not specifically mentioned), with slopes that followed the trend HCl > H_2SO_4 > H_3PO_4 (Fig. 2C), thus demonstrating the potential to screen acids.
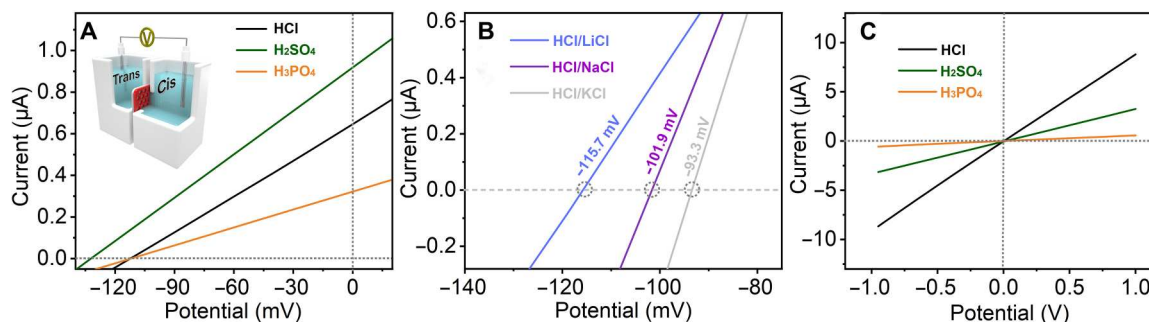
Fig. 2. Investigation of transmembrane ion transport. (**A**) Current-voltage relation (*I-V*) curves obtained for various asymmetric acid solutions with a concentration difference of 1000 (1 M/1 mM); inset: schematic of the experimental setup for electrochemical testing. (**B**) *I-V* curves recorded for asymmetrical electrolytes, with the *cis* side filled with KCl, NaCl, or LiCl aqueous solution and the *trans* side filled with HCl (0.1 M). Concentrations of Cl⁻ ions are maintained at 0.1 M. (**C**) *I-V* curves obtained with symmetrical acid solutions (0.1 M).

Evaluation of cation selectivity

The initial diffusion fluxes were measured on the basis of the rate determination average of three experiments to quantitatively calculate the transmembrane activity of protons and other cations across TpTag-COF/PAN. All these experiments involved an H-shaped diffusion cell in which the fabricated membrane was used to separate two aqueous solutions, and the feed and permeate reservoirs were filled with 30 ml of a chloride salt solution and deionized water, respectively (Fig. 3A). Single-ion diffusion profiles were collected with electrolyte concentrations ranging from 0.05 to 1 M. The number of permeating ions was recorded as a function of time using a conductivity meter or inductively coupled plasma optical emission spectrometry, in which the slope of the curves reflects the ion transport activity. The ion concentration in the permeate reservoir increased as the time and concentration of the feed solution increased (fig. S13). The permeances of various ions derived from the slope of the conductance-operation time curve revealed low ion conductivities over a wide range of electrolyte concentrations, except for HCl, illustrating the remarkable selectivity of TpTag-COF/PAN for protons. As a control experiment, the PAN membrane exhibited very high ion permeance for all ions tested and showed negligible selectivity (fig. S14), confirming the role of the COF active layer in ion screening. Figure S15 compares the transport rates of protons and other cations as a function of the feed concentration. The volcano-shaped curves obtained by plotting the selectivity against feed concentration imply that variations in the solution concentration result in large modulations in the membrane separation performance, with an optimal feed solution concentration of 0.25 M (Fig. 3B). At this concentration, the permeance of various cations ranged from 0.2 to 3.4 mmol m⁻² hour⁻¹. Combining the results of proton conductivity with those of other cations, maximum permeability ratios, $P(H^+)/P(M^{x+})$, of ~253, 259, 346, 886, 1116, 3545, and 4334 were obtained for H^+/K^+, H^+/Na^+, H^+/Li^+, H^+/Ca^{2+}, H^+/Mg^{2+}, H^+/Fe^{2+}, and H^+/Al^{3+}, respectively. These results indicate that TpTag-COF/PAN exhibits a selectivity trend of $K^+ > Na^+ > Li^+ > Ca^{2+} > Mg^{2+} > Fe^{2+} > Al^{3+}$, revealing monotonic decrease of permeation rates with increasing hydrated ion diameters and thus suggesting that the molecular sieving mechanism governed the cation selectivity of TpTag-COF/PAN (figs. S16 and S17). Therefore, a tentative mechanism for proton transport is proposed: Under the driving force of the concentration gradient, protons move in the direction of their concentration gradient from the feed solution to the permeation side. A high density of guanidinium moieties together with the possible hydrogen-bonded water chains in the one-dimensional pore channels provide carriers for fast proton transport across the membrane (*47*).

Evaluation of anion selectivity

Next, the performance of TpTag-COF/PAN as an anion filter was evaluated by performing tests on an equimolar premixed binary acid mixture. Figure 3 (C and D) demonstrates the selectivity profile of HCl relative to H_2SO_4 or H_3PO_4 in the permeate solution at various feed concentrations, with the maximum separation factors reaching 34 and 138 for HCl/H_2SO_4 and HCl/H_3PO_4, respectively. Figure S17 compares the maximum HCl/H_2SO_4 and HCl/H_3PO_4 transmembrane selectivities of TpTag-COF/PAN with those of the state-of-the-art ionic membranes (Nafion212 and Selemion AMVN), indicating that TpTag-COF/PAN far exceeds the selectivity of commercial membranes (fig. S18). In addition, permeation experiments were conducted at various temperatures to gain insights into the mechanism of the observed anion selectivity. The permeation rates of the tested acid (0.1 M) changed exponentially with the inverse of temperature, following the Arrhenius equation and yielding activation energies of 29.2, 47.8, and 74.3 kJ mol⁻¹ for HCl, H_2SO_4, and H_3PO_4, respectively (Fig. 3E; see details in the Supplementary Materials). These results confirmed that HCl molecules required less energy to diffuse across the membrane than H_2SO_4 and H_3PO_4, thereby leading to the observed selectivity (*48, 49*).

Mechanism investigation into the anion screening ability of TpTag-COF/PAN

Considering that the solvated radii decreased in the order of $SO_4^{2-} > Cl^- \approx H_nPO_4^{(3-n)-}$ (*50, 51*), a sieving effect due to steric hindrance may play an inconsequential role in the observed anion separation performance. We performed molecular dynamics (MD) simulations to provide an unbiased molecular-level description of various anions inside TpTag-COF/PAN. Radial distribution function calculations revealed that the relative distance of the anions to the oxygen species in TpTag-COF/PAN decreased in the order of HCl << H_2SO_4 < H_3PO_4 (Fig. 4A). Combining with the experimental transmembrane transport activities, these simulation results suggest that compared to the corresponding anion species of H_2SO_4 and H_3PO_4, the anion species of HCl forms a relative
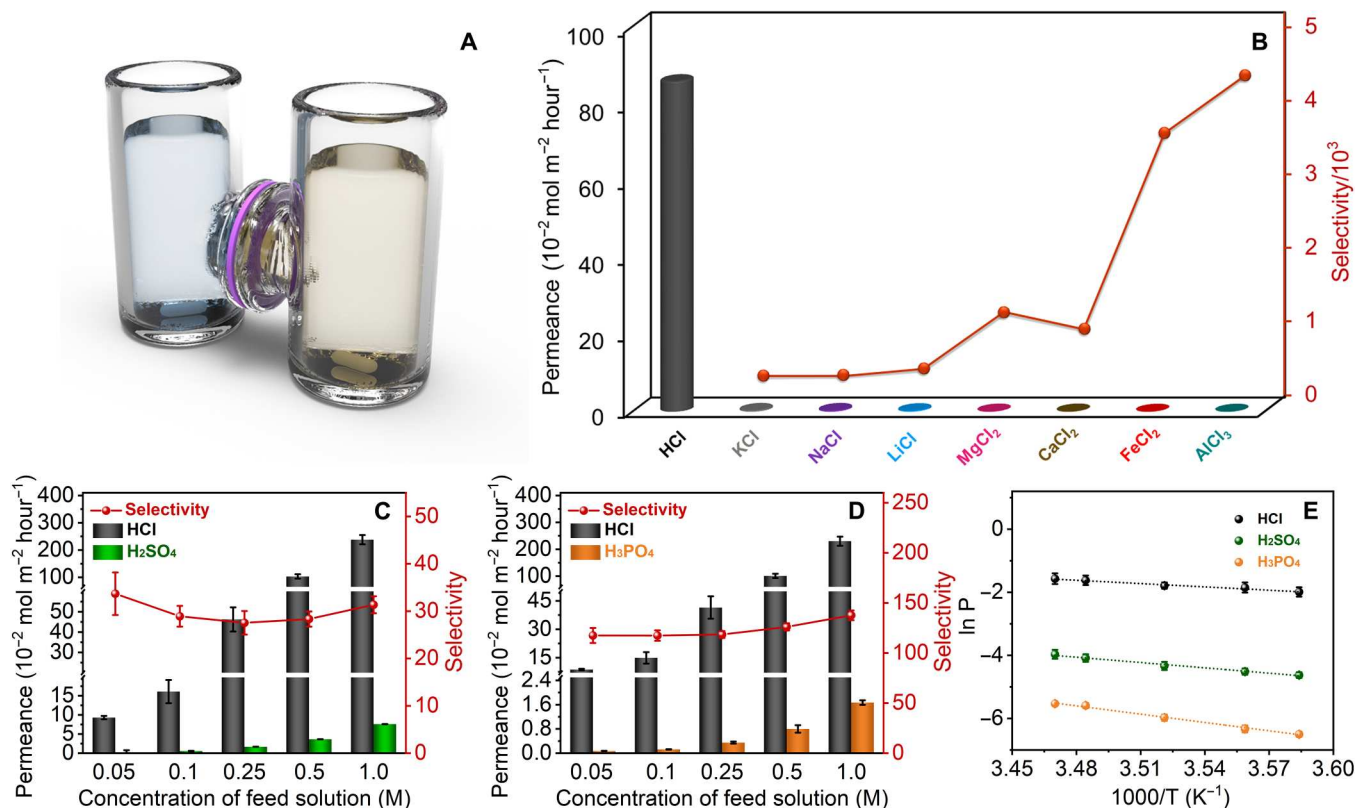
Fig. 3. Evaluation of cation and anion selectivity across TpTag-COF/PAN. (**A**) Schematic diagram of ion permeation through TpTag-COF/PAN (1,3,5-triformylphloroglucinol and triaminoguanidine hydrochloride–covalent organic framework/polyacrylonitrile) using an H-shaped diffusion cell. (**B**) Transport rate of various electrolytes across TpTag-COF/PAN and the corresponding H^+/M^{x+} selectivity obtained via diffusion dialysis using a concentration of 0.25 M. (**C** and **D**) Permeance of HCl, H_2SO_4, and H_3PO_4 and the corresponding selectivity of HCl to H_2SO_4 and H_3PO_4 across TpTag-COF/PAN, which were tested under binary acid conditions. (**E**) Acid permeation curves versus temperature across TpTag-COF/PAN and the corresponding Arrhenius plots. Error bars represent SD of three different measurements.

weaker association with TpTag-COF. To understand the anion-screening mechanism of TpTag-COF/PAN, two sets of additional experiments were conducted. First, MD simulations confirmed that the diffusion coefficient of HCl in TpTag-COF is substantially larger than that of H_2SO_4 and H_3PO_4 in TpTag-COF, affording the value of $0.1524 \pm 0.0501 \times 10^{-5}$, $0.0170 \pm 0.0079 \times 10^{-5}$, and $0.0080 \pm 0.0076 \times 10^{-5}$ cm^2 s^{-1} for HCl, H_2SO_4, and H_3PO_4, respectively (Fig. 4B). Second, considering the preferential complexation of TpTag-COF with H_2SO_4 and H_3PO_4, this may confer the pore channel of TpTag-COF with a more negative electrostatic potential (ESP). The ESP mapped on the van der Waals surface of TpTag-COF with various counter anions indicated that the negative partial charge along the pore content displayed a sequence of TpTag-COF/$H_2PO_4^-$ < TpTag-COF/HSO_4^- < TpTag-COF/Cl^- (fig. S19). Reduced zeta potentials of the membranes after anion exchange with Na_2SO_4 or Na_3PO_4 (−54.5 and −68.2 versus −9.0 mV) further validated the simulation results. These observations led to the possibility that ion rejection can be described using the Donnan model, in which the negatively charged pore surface repels coions, and the extent of repulsion is correlated with the extent of ion charge, thereby affording anion selectivity. Therefore, to demonstrate the importance of electrostatic repulsion on the observed separation, we evaluated the transport activity of HCl, H_2SO_4, and H_3PO_4 across TpTag-COF/PAN, and the corresponding separation factors in response to the feed concentration are summarized in figs. S20 to S22. A notable finding was the maintenance of HCl/H_3PO_4 and HCl/H_2SO_4 selectivity at various acid concentrations for TpTag-COF/PAN, contradicting the expectations based on electrostatic selectivity. This is because at high ionic strengths, the Debye length of solutions became smaller than the pore diameter of TpTag-COF/PAN, and therefore electrostatic repulsion does not contribute significantly to the solute rejection mechanism (52, 53). The acid permeance in response to concentration variation was investigated in detail to gain deeper insights into this observation. The transport of H_2SO_4 and H_3PO_4 was slow to initiate, which was evident by the slow realization of stability at low feed concentrations. H_2SO_4 and H_3PO_4 required up to 3 and 2.5 min, respectively, to attain stability before the conductivity increased monotonically, suggesting the strong association of H_2SO_4 and H_3PO_4 with the framework (fig. S23). After reaching stability, the transport of HCl, H_2SO_4, and H_3PO_4 is highly dependent on the bulk concentration, increasing proportionally with increasing concentration. These results lead us to conclude that the higher transport activity for HCl across TpTag-COF/PAN than that of H_2SO_4 and H_3PO_4 is strongly associated with its weaker host-guest interactions with the membrane because of kinetic selectivity.

Evaluation of acid separation performance
Considering that practical ion separation requires the recovery of a target ion from a concentrated solution, competitive interaction,
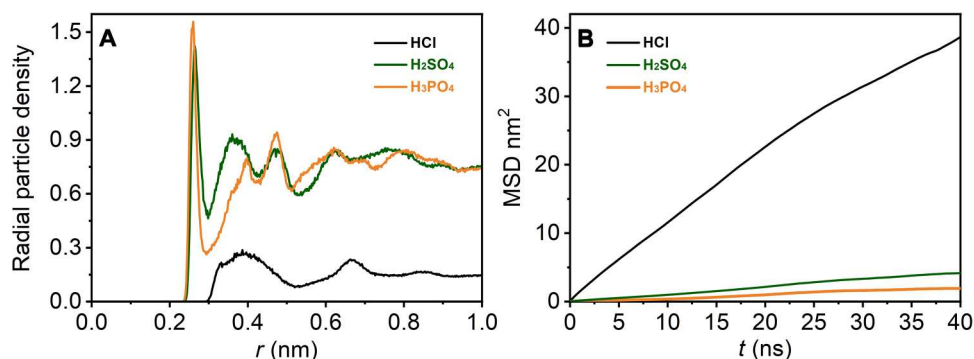
Fig. 4. MD calculation. (**A**) Relative distance of the anions to the oxygen species in TpTag-COF calculated according to the radial distribution function. (**B**) Diffusion coefficient of HCl, H_2SO_4, and H_3PO_4 across TpTag-COF. MSD, mean square deviation.

and flux coupling might influence ion selectivity in a nontrivial manner. We performed permeability measurements using equimolar solutions of HCl, H_2SO_4, and H_3PO_4 to investigate the preferential transport of TpTag-COF/PAN in mixed acid solutions. Furthermore, real-time fluxes of these acids were calculated to provide a comprehensive understanding of the process. The transport of HCl was consistently faster than that of the competitors, validating its higher diffusion ability across the membrane and affording HCl/H_2SO_4 and HCl/H_3PO_4 selectivities of 39 and 183, respectively (Fig. 5, A and B, and fig. S24). A comparison of the trinary- and single-component acid permeances indicates that the apparent permeabilities of HCl, H_2SO_4, and H_3PO_4 in the mixed system decreased relative to their single-component values, suggesting that the flux of each anion is coupled. To explain the discrepancy between single-component and multicomponent systems in terms of permeance, we reasoned that under mixed acid conditions, H_2SO_4 and H_3PO_4 with a strong association with TpTag-COF occupied the pore space and hence led to a decrease in diffusivity relative to corresponding single-acid conditions by competitive diffusion. The slightly decreased HCl/H_2SO_4 selectivity with increasing acid concentration can be explained as follows. The increased ion concentration difference across the membrane offers a strong driving force to enhance the transport activity of protons. Given the higher affinity of H_2SO_4 and H_3PO_4 toward the membrane, the pore channels are plugged with these compounds, leading to a decline in HCl penetration. However, the electroneutrality principle requires a concomitant increase in anion diffusivity, which promotes the transport of concentrated HSO_4^- in the pore

channel, thereby compromising the separation of HCl/H_2SO_4. The volcano-type curve of the HCl/H_3PO_4 selectivity can be attributed to the varying concentrations of the ionized H_3PO_4 species compromised by the dissociation equilibria in response to the increased concentrations of both H^+ and H_3PO_4. The former prevented the hydrolysis of H_3PO_4, while the latter shifted the equation in the opposite direction.

MD simulations were performed to further confirm these inferences. The simulation setup contained equal moles of acids (0.25 M) on one side of the four by four by five TpTag-COF layers. Starting from a random configuration, followed by a 1-fs production run, resulted in a set of trajectory files, revealing that the hydronium ions were the most preferred transport species. We further conducted a prolonged computational study of the >10-ns trajectory to gain additional computational insights into TpTag-COF–mediated selectivity for HCl, H_2SO_4, and H_3PO_4. Within a period of 10 ns, 12 Cl^- anions passed through the COF channel, and the other two anions traversed approximately one-third of the constructed COF layers (5.7 Å; Fig. 6). These results confirm the higher transport activity of HCl than that of H_2SO_4 and H_3PO_4 across the TpTag-COF channels when considering the neutrality requirement. The selective acid conduction at the molecular level involves the following steps: the formation of charge-assisted hydrogen bonding interactions with the membrane, separation of the charge carriers, migration, and subsequent neutralization.

Extraction of HCl from mixed waste

The TpTag-COF membrane with highly tunable exclusion abilities against polybasic acids and metal cations, while allowing free permeation of Cl^-, is a potential candidate for HCl recovery applications. To test the feasibility and long-term operational stability, the permeances of HCl, H_2SO_4, H_3PO_4, LiCl, NaCl, KCl, and $MgCl_2$ under equal molar conditions (0.1 M) and their relative selectivity toward HCl were plotted as a function of time. Notably, TpTag-COF/PAN displayed stable $P(HCl)/P(H_2SO_4)$ and $P(HCl)/P(H_3PO_4)$ selectivities of up to 149 and 437, respectively, together with the $P(HCl)/P(MCl_x)$ ratio of 1073/28,840, thereby indicating its unique prospects for the extraction of valuable chemicals from contaminants (Fig. 7, A and B). In addition, no noticeable alterations in the HCl extraction performance in terms of purity or flux were observed. The stable separation performance was corroborated using Fourier transform infrared (FTIR) spectroscopy, SEM,
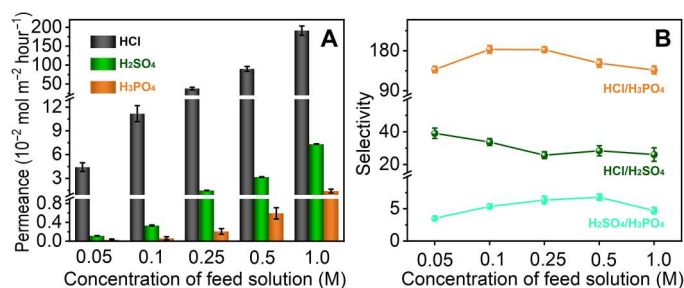

Fig. 5. Evaluation of acid separation performance across TpTag-COF/PAN. (**A**) Permeances of HCl, H_2SO_4, and H_3PO_4 and (**B**) their optimal relative selectivity across TpTag-COF/PAN in response to the feed concentration tested under trinary acid conditions (0.05, 0.1, 0.25, 0.5, and 1.0 M for each acid).
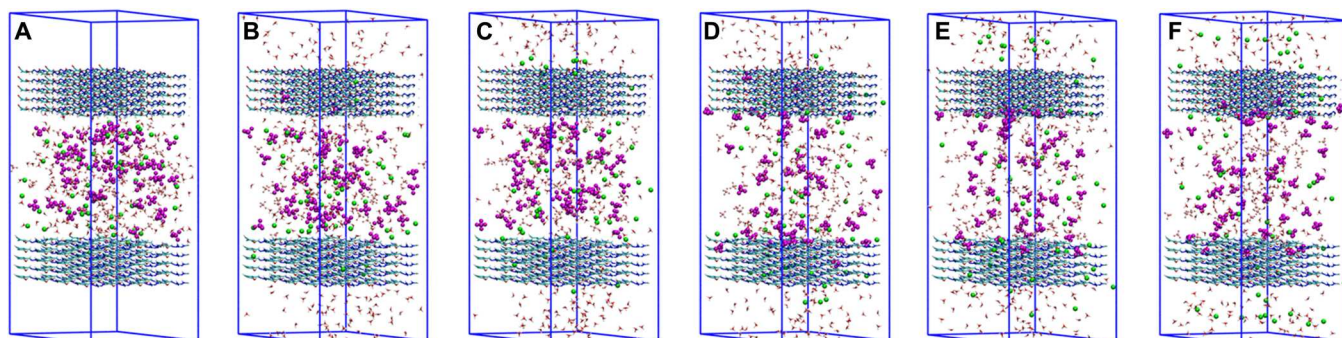
Fig. 6. Schematic diagram of various ion transport activities across TpTag-COF nanochannels. (**A**) 0, (**B**) 0.1, (**C**) 1, (**D**) 2, (**E**) 5, and (**F**) 10 ns. (Green, Cl^-; purple, PO_4^{3-}; gold, SO_4^{2-}; red, O; white, H; blue, TgTag-COF layers).
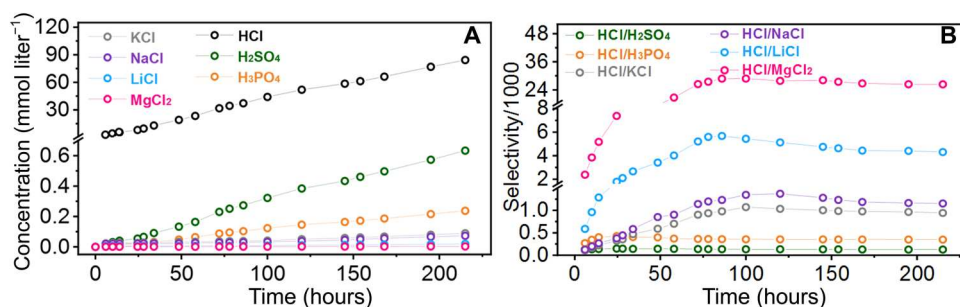

Fig. 7. HCl extraction from mixed wastes. (**A**) Permeance of various compounds through TpTag-COF/PAN (0.1 M each) to the permeate chamber and (**B**) corresponding separation factor as a function of time.

and PXRD analyses, showing the retained chemical structure, membrane morphology, and crystallinity (figs. S25 to S27).

DISCUSSION

In this study, we demonstrated that TpTag-COF/PAN with angstrom-sized porosity and implanted charge-assisted hydrogen bond donors produced pores capable of the selective extraction of HCl from complex mixtures. The angstrom-sized pores of TpTag-COF/PAN could effectively sieve protons from other cations with a selectivity of up to 4334. The difference in the charge-assisted hydrogen bond donation abilities of the guanidinium moieties toward various anions enables the membrane to serve as an anion filter. HCl with a relatively weaker affinity toward the membrane are easier to dissociate for surface jumping and fast diffusion. With these attributes, TpTag-COF/PAN exhibited outstanding performance in HCl mining from mixed waste containing a variety of cations and anions. The unprecedented ion selectivity of TpTag-COF/PAN presents a valuable paradigm that would contribute significantly to precise separation.

MATERIALS AND METHODS

Commercially available reagents were purchased in high purity and used without purification. The synthetic procedures of the COF membrane are detailed in the supplementary text. The asymmetric PAN ultrafiltration membrane was obtained from Sepro Membranes Inc. (Carlsbad, CA, USA) with a molecular weight cutoff of 50,000 Da. PXRD data were collected on a Bruker AXS D8

Advance A25 powder x-ray diffractometer (40 kV, 40 mA) using Cu Kα (λ = 1.5406 Å) radiation. SEM was performed on a Hitachi SU8000. The gas adsorption isotherms were collected on the surface area analyzer ASAP 2020. The N_2 sorption isotherms were measured at 77 K using a liquid N_2 bath. FTIR spectra were recorded on a Nicolet Impact 410 FTIR spectrometer. The surface charge distribution of the membranes was investigated by means of zeta potential. Surface zeta potentials of the composite membrane were obtained using a streaming potential analyzer (SurPASS, Aaton Paar, Austria). Membrane samples were cut into 1 cm by 2 cm by a cutter and taped on the measuring cell using adhesive tape. Measurements were carried out with KCl aqueous solution (1.0 mmol liter^{-1}) at (25.0 ± 1.0)°C at a pH of 6.5. Data were collected for four cycles at each measuring point. Surface zeta potential was calculated according to the Helmholtz-Smoluchowski equation.

Supplementary Materials

This PDF file includes:
Figs. S1 to S28
Table S1
Supplementary Text
References

REFERENCES AND NOTES

1. A. Halder, S. Karak, M. Addicoat, S. Bera, A. Chakraborty, S. H. Kunjattu, P. Pachfule, T. Heine, R. Banerjee, Ultrastable imine-based covalent organic frameworks for sulfuric acid recovery: An effect of interlayer hydrogen bonding. *Angew. Chem. Int. Ed.* **57**, 5797–5802 (2018).

2. X. Lin, E. Shamsaei, B. Kong, J. Z. Liu, T. Xu, H. Wang, Fabrication of asymmetrical diffusion dialysis membranes for rapid acid recovery with high purity. *J. Mater. Chem. A* **3**, 24000–24007 (2015).

3. W. Song, Y. He, M. A. Shehzad, X. Ge, L. Ge, X. Liang, C. Wei, Z. Ge, K. Zhang, G. Li, W. Yu, L. Wu, T. Xu, Exploring H-bonding interaction to enhance proton permeability of an acid-selective membrane. *J. Membr. Sci.* **637**, 119650 (2021).

4. A. Agrawal, K. K. Sahu, An overview of the recovery of acid from spent acidic solutions from steel and electroplating industries. *J. Hazard. Mater.* **171**, 61–75 (2009).

5. G. Naidu, S. Ryu, R. Thiruvenkatachari, Y. Choi, S. Jeong, S. Vigneswaran, A critical review on remediation, reuse, and resource recovery from acid mine drainage. *Environ. Pollut.* **247**, 1110–1124 (2019).

6. S. Yuan, X. Li, J. Zhu, G. Zhang, P. Van Puyvelde, B. Van der Bruggen, Covalent organic frameworks for membrane separation. *Chem. Soc. Rev.* **48**, 2665–2681 (2019).

7. Y. Cai, D. Chen, N. Li, Q. Xu, H. Li, J. He, J. Lu, A self-cleaning heterostructured membrane for efficient oil-in-water emulsion separation with stable flux. *Adv. Mater.* **32**, 2001265 (2020).

8. B. H. Monjezi, K. Kutonova, M. Tsotsalas, S. Henke, A. Knebel, Current trends in metal-organic and covalent organic framework membrane materials. *Angew. Chem. Int. Ed.* **60**, 15153–15164 (2021).

9. Y. Li, Q. Wu, X. Guo, M. Zhang, B. Chen, G. Wei, X. Li, X. Li, S. Li, L. Ma, Laminated self-standing covalent organic framework membrane with uniformly distributed subnanopores for ionic and molecular sieving. *Nat. Commun.* **11**, 599 (2020).

10. C. Zhang, B.-H. Wu, M.-Q. Ma, Z. Wang, Z.-K. Xu, Ultrathin metal/covalent-organic frame-work membranes towards ultimate separation. *Chem. Soc. Rev.* **48**, 3811–3841 (2019).

11. Y. Liu, W. Zhou, W. L. Teo, K. Wang, L. Zhang, Y. Zeng, Y. Zhao, Covalent-organic-framework-based composite materials. *Chem* **6**, 3172–3202 (2020).

12. H. Fan, J. Gu, H. Meng, A. Knebel, J. Caro, High-flux membranes based on the covalent organic framework COF-LZU1 for selective dye separation by nanofiltration. *Angew. Chem. Int. Ed.* **57**, 4083–4087 (2018).

13. R. Zhang, Y. Liu, M. He, Y. Su, X. Zhao, M. Elimelech, Z. Jiang, Antifouling membranes for sustainable water purification: Strategies and mechanisms. *Chem. Soc. Rev.* **45**, 5888–5924 (2016).

14. S. Ling, Z. Qin, W. Huang, S. Cao, D. L. Kaplan, M. J. Buehler, Design and function of bio-mimetic multilayer water purification membranes. *Sci. Adv.* **3**, e1601939 (2017).

15. G. He, R. Zhang, Z. Jiang, Engineering covalent organic framework membranes. *Acc. Mater. Res.* **2**, 630–643 (2021).

16. K. Tiwari, P. Sarkar, S. Modak, H. Singh, S. K. Pramanik, S. Karan, A. Das, Large area self-assembled ultrathin polyimine nanofilms formed at the liquid-liquid interface used for molecular separation. *Adv. Mater.* **32**, 1905621 (2020).

17. Z. Zhang, X. Shi, R. Wang, A. Xiao, Y. Wang, Ultra-permeable polyamide membranes harvested by covalent organic framework nanofiber scaffolds: a two-in-one strategy. *Chem. Sci.* **10**, 9077–9083 (2019).

18. V. A. Kuehl, J. Yin, P. H. H. Duong, B. Mastorovich, B. Newell, K. D. Li-Oakey, B. A. Parkinson, J. O. Hoberg, A highly ordered nanoporous, two-dimensional covalent organic framework with modifiable pores, and its application in water purification and ion sieving. *J. Am. Chem. Soc.* **140**, 18200–18207 (2018).

19. D. B. Shinde, G. Sheng, X. Li, M. Ostwal, A. H. Emwas, K. W. Huang, Z. Lai, Crystalline 2D covalent organic framework membranes for high-flux organic solvent nanofiltration. *J. Am. Chem. Soc.* **140**, 14342–14349 (2018).

20. X. You, H. Wu, R. Zhang, Y. Su, L. Cao, Q. Yu, J. Yuan, K. Xiao, M. He, Z. Jiang, Metal-coordinated sub-10 nm membranes for water purification. *Nat. Commun.* **10**, 4160 (2019).

21. A. He, Z. Jiang, Y. Wu, H. Hussain, J. Rawle, M. E. Briggs, M. A. Little, A. G. Livingston, A. I. Cooper, A smart and responsive crystalline porous organic cage membrane with switchable pore apertures for graded molecular sieving. *Nat. Mater.* **21**, 463–470 (2022).

22. F. Sun, F. Yi, R.-H. Li, X. Min, H. Qin, S.-Q. Cheng, Y. Liu, Inorganic-organic hybrid membrane based on pillararene-intercalated MXene nanosheets for efficient water purification. *Angew. Chem. Int. Ed.* **61**, e202200482 (2022).

23. S. Zhao, C. Jiang, J. Fan, S. Hong, P. Mei, R. Yao, Y. Liu, S. Zhang, H. Li, H. Zhang, C. Sun, Z. Guo, P. Shao, Y. Zhu, J. Zhang, L. Guo, Y. Ma, J. Zhang, X. Feng, F. Wang, H. Wu, B. Wang, Hydrophilicity gradient in covalent organic frameworks for membrane distillation. *Nat. Mater.* **20**, 1551–1558 (2021).

24. Y. Wang, Y. He, Q. Wang, X. Wang, B. L. Tardy, J. J. Richardson, O. J. Rojas, J. Guo, Micro-porous membranes for ultrafast and energy-efficient removal of antibiotics through polyphenol-mediated nanointerfaces. *Matter* **6**, 260–273 (2023).

25. C. Wu, Y. Wu, J. Luo, T. Xu, Y. Fu, Anion exchange hybrid membranes from PVA and multi-alkoxy silicon copolymer tailored for diffusion dialysis process. *J. Membr. Sci.* **356**, 96–104 (2010).

26. A. N. Mondal, C. Cheng, Z. Yao, J. Pan, M. M. Hossain, M. I. Khan, Z. Yang, L. Wu, T. Xu, Novel quaternized aromatic amine based hybrid PVA membranes for acid recovery. *J. Membr. Sci.* **490**, 29–37 (2015).

27. C. Yang, L. Hou, J. Zhao, Z. Yao, G. Li, L. Zhang, L. Hou, Cationic covalent organic framework membranes with stable proton transfer channel for acid recovery. *Chem. Eng. J.* **428**, 131124 (2022).

28. S.-P. Zheng, L.-B. Huang, Z. Sun, M. Barboiu, Self-assembled artificial ion-channels toward natural selection of functions. *Angew. Chem. Int. Ed.* **60**, 566–597 (2021).

29. X. Li, B. Shen, X.-Q. Yao, D. Yang, A small synthetic molecule forms chloride channels to mediate chloride transport across cell membranes. *J. Am. Chem. Soc.* **129**, 7264–7265 (2007).

30. C. R. Martin, Z. S. Siwy, Learning nature's way: Biosensing with synthetic nanopores. *Science* **317**, 331–332 (2007).

31. D. A. Doyle, J. M. Cabral, R. A. Pfuetzner, A. Kuo, J. M. Gulbis, S. L. Cohen, B. T. Chait, R. MacKinnon, The structure of the potassium channel: Molecular basis of K+ conduction and selectivity. *Science* **280**, 69–77 (1998).

32. H. Xie, V. W. L. Gunawardana, T. J. Finnegan, W. Xie, J. D. Badjić, Picking on carbonate: Kinetic selectivity in the encapsulation of anions. *Angew. Chem. Int. Ed.* **61**, e202116518 (2022).

33. C. F. Guerra, F. M. Bickelhaupt, J. G. Snijders, E. J. Baerends, The nature of the hydrogen bond in DNA base pairs: The role of charge transfer and resonance assistance. *Chem. A Eur. J.* **5**, 3581–3594 (1999).

34. J. Jasti, H. Furukawa, E. B. Gonzales, E. Gouaux, Structure of acid-sensing ion channel 1 at 1.9 Å resolution and low pH. *Nature* **449**, 316–323 (2007).

35. X. Wu, A. M. Gilchrist, P. A. Gale, Prospects and challenges in anion recognition and transport. *Chem* **6**, 1296–1309 (2020).

36. X. Ji, X. Chi, M. Ahmed, L. Long, J. L. Sessler, Soft materials constructed using calix[4]pyr-role- and "texas-sized" box-based anion receptors. *Acc. Chem. Res.* **52**, 1915–1927 (2019).

37. X. Li, H. Zhang, H. Yu, J. Xia, Y. -B. Zhu, H. -A. Wu, J. Hou, J. Lu, R. Ou, C. D. Easton, C. Selomulya, M. R. Hill, L. Jiang, H. Wang, Unidirectional and selective proton transport in artificial heterostructured nanochannels with nano-to-subnano confined water clusters. *Adv. Mater.* **32**, 2001777 (2020).

38. G. Park, F. P. Gabbaï, F. P., Phosphonium boranes for the selective transport of fluoride anions across artificial phospholipid membranes. *Angew. Chem. Int. Ed.* **59**, 5298–5302 (2020).

39. J. Shen, J. Fan, R. Ye, N. Li, Y. Mu, H. Zeng, Polypyridine-based helical amide foldamer channels: Rapid transport of water and protons with high ion rejection. *Angew. Chem. Int. Ed.* **59**, 13328–13334 (2020).

40. Y. Guo, Z. Jiang, W. Ying, L. Chen, Y. Liu, X. Wang, Z.-J. Jiang, B. Chen, X. Peng, A DNA-threaded ZIF-8 membrane with high proton conductivity and low methanol permeability. *Adv. Mater.* **30**, 1705155 (2018).

41. H. Zhang, X. Li, J. Hou, L. Jiang, H. Wang, Angstrom-scale ion channels towards single-ion selectivity. *Chem. Soc. Rev.* **51**, 2224–2254 (2022).

42. X. Li, H. Zhang, J. Hou, R. Ou, Y. Zhu, C. Zhao, T. Qian, C. D. Easton, C. Selomulya, M. R. Hill, H. Wang, Sulfonated sub-1-nm metal-organic framework channels with ultrahigh proton selectivity. *J. Am. Chem. Soc.* **142**, 9827–9833 (2020).

43. I. Rozas, I. Alkorta, J. Elguero, Hydrogen bonds and ionic interactions in guanidine/gua-nidinium complexes: A computational case study. *Struct. Chem.* **19**, 923–933 (2008).

44. P. Zhang, S. Chen, C. Zhu, L. Hou, W. Xian, X. Zuo, Q. Zhang, L. Zhang, S. Ma, Q. Sun, Co-valent organic framework nanofluidic membrane as a platform for highly sensitive bionic thermosensation. *Nat. Commun.* **12**, 1844 (2021).

45. C. Zhu, W. Xian, Y. Song, X. Zuo, Y. Wang, S. Ma, Q. Sun, Manipulating charge density in nanofluidic membranes for optimal osmotic energy production density. *Adv. Funct. Mater.* **32**, 2109210 (2022).

46. W.-L. Huang, X.-D. Wang, Y.-F. Ao, Q.-Q. Wang, D.-X. Wang, Artificial chloride-selective channel: Shape and function mimic of the ClC channel selective pore. *J. Am. Chem. Soc.* **142**, 13273–13277 (2020).

47. G. Chen, L. Ge, J. H. Lee, Z. Zhu, H. Wang, Porous coordination polymer-based composite membranes for high-temperature polymer exchange membrane fuel cells. *Matter* **5**, 2031–2053 (2022).

48. J. Abraham, K. S. Vasu, C. D. Williams, K. Gopinadhan, Y. Su, C. T. Cherian, J. Dix, E. Prestat, S. J. Haigh, I. V. Grigorieva, P. Carbone, A. K. Geim, R. R. Nair, Tunable sieving of ions using graphene oxide membranes. *Nat. Nanotechnol.* **12**, 546–550 (2017).

49. X. Zuo, C. Zhu, W. Xian, Q.-W. Meng, Q. Guo, X. Zhu, S. Wang, Y. Wang, S. Ma, Q. Sun, Thermo-osmotic energy conversion enabled by covalent-organic-framework membranes with record output power density. *Angew. Chem. Int. Ed.* **61**, e202116910 (2022).

50. B. Tansel, J. Sager, T. Rector, J. Garland, R. F. Strayer, L. Levine, M. Roberts, M. Hummerick, J. Bauer, Significance of hydrated radius and hydration shells on ionic permeability during nanofiltration in dead end and cross flow modes. *Sep. Purif. Technol.* **51**, 40–47 (2006).

51. Y. Zhao, T. Tong, X. Wang, S. Lin, E. M. Reid, Y. Chen, Differentiating solutes with precise nanofiltration for next generation environmental separations: A review. *Environ. Sci. Technol.* **55**, 1359–1376 (2021).

52. Y. Tanaka, Chapter 7 Donnan dialysis. *Membr. Sci. Technol.* **12**, 495–453 (2007).

53. Y.-X. Shen, W. Song, D. R. Barden, T. Ren, C. Lang, H. Feroz, C. B. Henderson, P. O. Saboe, D. Tsai, H. Yan, P. J. Butler, G. C. Bazan, W. A. Phillip, R. J. Hickey, P. S. Cremer, H. Vashisth, M. Kumar, Achieving high permeability and enhanced selectivity for angstrom-scale separations using artificial water channel membranes. *Nat. Commun.* **9**, 2294 (2018).

54. S. Mitra, S. Kandambeth, B. P. Biswal, A. M. Khayum, C. K. Choudhury, M. Mehta, G. Kaur, S. Banerjee, A. Prabhune, S. Verma, S. Roy, U. K. Kharul, R. Banerjee, Self-exfoliated gua-nidinium-based ionic covalent organic nanosheets (iCONs). *J. Am. Chem. Soc.* **138**, 2823–2828 (2016).

55. Y. Zhao, N. Mamrol, W. A. Tarpeh, X. Yang, C. Gao, B. Van der Bruggen, Advanced ion transfer materials in electro-driven membrane processes for sustainable ion-resource ex-traction and recovery. *Prog. Mater. Sci.* **128**, 100958 (2022).

56. L. Chen, G. Shi, J. Shen, B. Peng, B. Zhang, Y. Wang, F. Bian, J. Wang, D. Li, Z. Qian, G. Xu, G. Liu, J. Zeng, L. Zhang, Y. Yang, G. Zhou, M. Wu, W. Jin, J. Li, H. Fang, Ion sieving in graphene oxide membranes via cationic control of interlayer spacing. *Nature* **550**, 380–383 (2017).

57. S. Cong, Y. Yuan, J. Wang, Z. Wang, F. Kapteijn, X. Liu, Highly water-permeable metal-organic framework MOF-303 membranes for desalination. *J. Am. Chem. Soc.* **143**, 20055–20058 (2021).

58. W. Xin, J. Fu, Y. Qian, L. Fu, X.-Y. Kong, T. Ben, L. Jiang, L. Wen, Biomimetic KcsA channels with ultra-selective K$^+$ transport for monovalent ion sieving. *Nat. Commun.* **13**, 1701 (2022).

59. A. Razmjou, M. Asadnia, E. Hosseini, A. Habibnejad Korayem, V. Chen, Design principles of ion selective nanostructured membranes for the extraction of lithium ions. *Nat. Commun.* **10**, 5793 (2019).

60. X. Liu, N. K. Demir, Z. Wu, K. Li, Highly water-stable zirconium metal-organic framework UiO-66 membranes supported on alumina hollow fibers for desalination. *J. Am. Chem. Soc.* **137**, 6999–7002 (2015).

61. V. Chavan, C. Agarwal, V. C. Adya, A. K. Pandey, Hybrid organic-inorganic anion-exchange pore-filled membranes for the recovery of nitric acid from highly acidic aqueous waste streams. *Water Res.* **133**, 87–98 (2018).

62. J. D. Lear, Z. R. Wasserman, W. F. DeGrado, Synthetic amphiphilic peptide models for protein ion channels. *Science* **240**, 1177–1181 (1988).

63. W. Xia, Y. Yang, X. Shang, X. Yang, S. Wang, F. Gong, L. Wang, X. Wang, X. Chen, Cardo-poly(arylene ether sulfone)s membranes bearing N-cyclic cationic groups enable high performance during both diffusion dialysis and electrodialysis. *Desalination* **529**, 115646 (2022).

64. R. Mondal, S. Pal, U. Chatterjee, Alkylated imidazole moieties in a cross-linked anion ex-change membrane facilitate acid recovery with high purity. *ACS Appl. Polym. Mater.* **3**, 1544–1554 (2021).

65. M. Irfan, E. Bakangura, N. U. Afsar, T. Xu, Augmenting acid recovery from different systems by novel Q-DAN anion exchange membranes via diffusion dialysis. *Sep. Purif. Technol.* **201**, 336–345 (2018).

66. W. Ji, X. Ge, N. U. Afsar, Z. Zhao, B. Wu, W. Song, Y. He, L. Ge, T. Xu, In-situ crosslinked AEMs with self-assembled nanostructure for acid recovery. *Sep. Purif. Technol.* **247**, 116927 (2020).

67. L. Ge, A. N. Mondal, X. Liu, B. Wu, D. Yu, Q. Li, J. Miao, Q. Ge, T. Xu, Advanced charged porous membranes with ultrahigh selectivity and permeability for acid recovery. *J. Membr. Sci.* **536**, 11–18 (2017).

68. C. Yang, L. Hou, T. Yao, J. Zhao, L. Hou, L. Zhang, High proton selectivity membrane based on the keto-linked cationic covalent organic framework for acid recovery. *J. Membr. Sci.* **640**, 119800 (2021).

69. C. Yang, L. Hou, J. Zhao, Z. Yao, G. Li, L. Zhang, L. Hou, Cationic covalent organic framework membranes with stable proton transfer channel for acid recovery. *Chem. Eng. J.* **428**, 1535–1542 (2019).

70. X. Zhu, X. Cheng, X. Luo, Y. Liu, D. Xu, X. Tang, Z. Gan, L. Yang, G. Li, H. Liang, Ultrathin thin-film composite polyamide membranes constructed on hydrophilic poly(vinyl alcohol) decorated support toward enhanced nanofiltration performance. *Environ. Sci. Technol.* **54**, 6365–6374 (2020).

71. F. Fornasiero, H. G. Park, J. K. Holt, M. Stadermann, C. P. Grigoropoulos, A. Noy, O. Bakajin, Ion exclusion by sub-2-nm carbon nanotube pores. *Proc. Natl. Acad. Sci. U.S.A.* **105**, 17250–17255 (2008).

72. X. Wei, S. Wang, Y. Shi, H. Xiang, Application of positively charged composite hollow-fiber nanofiltration membranes for dye purification. *Ind. Eng. Chem. Res.* **53**, 14036–14045 (2014).

73. Z. Yang, Z.-W. Zhou, H. Guo, Z. Yao, X.-H. Ma, X. Song, S.-P. Feng, C. Y. Tang, Tannic acid/Fe^{3+} nanoscaffold for interfacial polymerization: Toward enhanced nanofiltration performance. *Environ. Sci. Technol.* **52**, 9341–9349 (2018).

74. Z. Wang, Z. Wang, S. Lin, H. Jin, S. Gao, Y. Zhu, J. Jin, Nanoparticle-templated nanofiltration membranes for ultrahigh performance desalination. *Nat. Commun.* **9**, 2004 (2018).

75. S. Gao, Y. Zhu, Y. Gong, Z. Wang, W. Fang, J. Jin, Ultrathin polyamide nanofiltration membrane fabricated on brush-painted single-walled carbon nanotube network support for ion sieving. *ACS Nano* **13**, 5278–5290 (2019).

76. A. Pérez-González, R. Ibáñez, P. Gómez, A. M. Urtiaga, I. Ortiz, J. A. Irabien, Nanofiltration separation of polyvalent and monovalent anions in desalination brines. *J. Membr. Sci.* **473**, 16–27 (2015).

77. Z. Tan, S. Chen, X. Peng, L. Zhang, C. Gao, Polyamide membranes with nanoscale turing structures for water purification. *Science* **360**, 518–521 (2018).

78. Y. Yang, X. Yang, L. Liang, Y. Gao, H. Cheng, X. Li, M. Zou, R. Ma, Q. Yuan, X. Duan, Large-area graphene-nanomesh/carbon-nanotube hybrid membranes for ionic and molecular nanofiltration. *Science* **364**, 1057–1062 (2019).

79. H. Zhang, X. Quan, X. Fan, G. Yi, S. Chen, H. Yu, Y. Chen, Improving ion rejection of con-ductive nanofiltration membrane through electrically enhanced surface charge density. *Environ. Sci. Technol.* **53**, 868–877 (2019).

80. J. Pan, J. Ding, R. Tan, G. Chen, Y. Zhao, C. Gao, B. Van der Bruggen, J. Shen, Preparation of a monovalent selective anion exchange membrane through constructing a covalently crosslinked interface by electro-deposition of polyethyleneimine. *J. Membr. Sci.* **539**, 263–272 (2017).

81. Y. Zhang, R. Liu, Q. Lang, M. Tan, Y. Zhang, Composite anion exchange membrane made by layer-by-layer method for selective ion separation and water migration control. *Sep. Purif. Technol.* **192**, 278–286 (2018).

82. M. Li, W. Li, X. Zhang, C. Wu, X. Han, Y. Chen, Polyvinyl alcohol-based monovalent anion selective membranes with excellent permselectivity in selectrodialysis. *J. Membr. Sci.* **620**, 118889 (2021).

83. J. Pan, J. Ding, Y. Zheng, C. Gao, B. Van der Bruggen, J. Shen, One-pot approach to prepare internally cross-linked monovalent selective anion exchange membranes. *J. Membr. Sci.* **553**, 43–53 (2018).

84. J. Liao, J. Zhu, S. Yang, N. Pan, X. Yu, C. Wang, J. Li, J. Shen, Long-side-chain type imida-zolium-functionalized fluoro-methyl poly(arylene ether ketone) anion exchange mem-branes with superior electrodialysis performance. *J. Membr. Sci.* **574**, 181–195 (2019).

85. Y. Zhao, Y. Li, S. Yuan, J. Zhu, S. Houtmeyers, J. Li, R. Dewil, C. Gao, B. Van der Bruggen, A chemically assembled anion exchange membrane surface for monovalent anion selectivity and fouling reduction. *J. Mater. Chem. A* **7**, 6348–6356 (2019).

86. M. Irfan, L. Ge, Y. Wang, Z. Yang, T. Xu, Hydrophobic side chains impart anion exchange membranes with high monovalent-divalent anion selectivity in electrodialysis. *ACS Sus-tainable Chem. Eng.* **7**, 4429–4442 (2019).

87. L. Shen, R. Cheng, M. Yi, W.-S. Hung, S. Japip, L. Tian, X. Zhang, S. Jiang, S. Li, Y. Wang, Polyamide-based membranes with structural homogeneity for ultrafast molecular sieving. *Nat. Commun.* **13**, 500 (2022).

88. M. Su, D.-X. Wang, X.-L. Wang, M. Ando, T. Shintani, Rejection of ions by NF membranes for binary electrolyte solutions of NaCl, NaNO$_3$, CaCl$_2$ and Ca(NO$_3$)$_2$. *Desalination* **191**, 303–308 (2006).

89. L. Zhou, X. Li, K. Cao, Z. Jia, H. Long, Y. Li, G. Tao, N. Liu, J. Zhang, L. Ma, Covalent organic framework membrane with turing structures for deacidification of highly acidic solutions. *Adv. Funct. Mater.* **32**, 2108178 (2022).

90. T. Lu, Molclus program, version 1.9.9.7 (2022); www.keinsci.com/research/molclus.html.

91. J. J. P. Stewart, Mopac: A semiempirical molecular orbital program. *J. Comput. Aided Mol. Des.* **4**, 1–103 (1990).

92. M. J. Frisch, G. W. Trucks, H. B. Schlegel, G. E. Scuseria, M. A. Robb, J. R. Cheeseman, G. Scalmani, V. Barone, B. Mennucci, G. A. Petersson, H. Nakatsuji, M. Caricato, X. Li, H. P. Hratchian, A. F. Izmaylov, G. Zheng, J. L. Sonnenberg, M. Hada, M. Ehara, K. Toyota, R. Fukuda, J. Hasegawa, M. Ishida, T. Nakajima, Y. Honda, O. Kitao, H. Nakai, T. Vreven, J. A. Montgomery, Jr., J. E. Peralta, F. Ogliaro, M. Bearpark, J. J. Heyd, E. Brothers, K. N. Kudin, V. N. Staroverov, R. Kobayashi, J. Normand, K. Raghavachari, A. Rendell, J. C. Burant, S. S. Iyengar, J. Tomasi, M. Cossi, N. Rega, J. M. Millam, M. Klene, J. E. Knox, J. B. Cross, V. Bakken, C. Adamo, J. Jaramillo, R. Gomperts, R. E. Stratmann, O. Yazyev, A. J. Austin, R. Cammi, C. Pomelli, J. W. Ochterski, R. L. Martin, K. Morokuma, V. G. Zakrzewski, G. A. Voth, P. Salvador, J. J. Dannenberg, S. Dapprich, A. D. Daniels, Ö. Farkas, J. B. Foresman, J. V. Ortiz, J. Cioslowski, D. J. Fox, Gaussian 09, Revision E.01: Wallingford CT (2009).

93. T. Lu, F. Chen, Multiwfn: A multifunctional wavefunction analyzer. *J. Comput. Chem.* **33**, 580–592 (2012).

94. W. Humphrey, A. Dalke, K. Schulten, VMD: Visual molecular dynamics. *J. Mol. Graph.* **14**, 33–38 (1996).

95. B. Hess, C. Kutzner, D. V. D. Spoel, E. Lindahl, GROMACS 4: Algorithms for highly efficient, load-balanced, and scalable molecular simulation. *J. Chem. Theory Comput.* **4**, 435–447 (2008).

96. K. G. Sprenger, V. W. Jaeger, J. Pfaendtner, The general AMBER force field (GAFF) can accurately predict thermodynamic and transport properties of many ionic liquids. *J. Phys. Chem. B* **119**, 5882–5895 (2015).

97. J. Wang, R. M. Wolf, J. W. Caldwell, P. A. Kollman, D. A. Case, Development and testing of a general amber force field. *J. Comput. Chem.* **25**, 1157–1174 (2004).

98. U. Essmann, L. Perera, M. L. Berkowitz, T. Darden, H. Lee, L. G. Pedersen, A smooth particle mesh Ewald method. *J. Chem. Phys.* **103**, 8577–8593 (1995).

99. B. Hess, H. Bekker, H. J. C. Berendsen, J. G. E. M. Fraaije, LINCS: A linear constraint solver for molecular simulations. *J. Comput. Chem.* **18**, 1463–1472 (1997).